Application of Convolutional Dendrite Net for Detection of Myocardial Infarction Using ECG Signals

Xin Ma, *Member, IEEE*, Xingwen Fu, Yiqi Sun, Nan Wang, and Yang Gao

***Abstract*—Myocardial infarction (MI) is a sudden-onset medical emergency. Without timely diagnosis and treatment, mortality is very high. The mining of deep features increases the computational burden while improving the accuracy of MI detection. So, there is a trade-off between speed and accuracy. However, considering our own classification process, we are more inclined to integrate the logic between shallow features and deep features. Therefore, this article is dedicated to transforming the high computational cost deep features into low computational cost shallow feature logic, so as to improve the speed without affecting the accuracy. The method proposed in this article mainly includes artifact removal, waveform location, coding, and classification. Hilbert curve completes the coding, which efficiently converts the time-domain features of electrocardiogram (ECG) signals into image features through a double recursive algorithm. Convolutional Dendrite Net (CDD Net) realizes the classification of images by extracting the logical relationship between features. The method is verified by Physikalisch Technische Bundesanstalt (PTB) dataset. The results show that the average detection accuracy and time of one patient are 98.95% and 2.09 ms, respectively.**

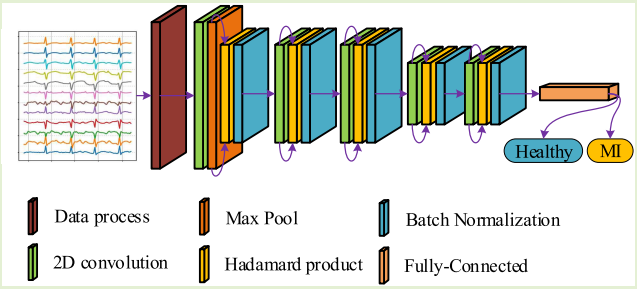

***Index Terms*—Artificial neural networks (ANNs), coding of Hilbert curve, convolutional dendrite net (CDD Net), electrocardiogram (ECG) signal processing, myocardial infarction (MI).**

NOMENCLATURE

Acc	Accuracy.
ARB-Net	Attentive RNN-based network.
ANN	Artificial neural network.
BW	Baseline wander.
CDD	Convolutional dendritic model.
CDD Net	Convolutional dendrite net.
CHD	Coronary heart disease.
CK-MB	Creatine kinase MB.
CNN	Convolutional neural networks.
DD	Dendritic net.
DCNN	Deep convolutional neural networks.
ECG	Electrocardiogram.
EDN	ECG-Deep-NET.
EMG	Electromyogram.
FN	False negative.
FP	False positive.
GHE	Global Health Estimates.
GMMs	Gaussian mixture models.
IHD	Ischemic heart disease.
HMMs	Hidden Markov models.
KNN	K-nearest neighbor.
MCG	Magnetocardiography.
MFB-CNN	Multiple-feature-branch convolutional neural networks.
MI	Myocardial infarction.
MLP	Multilayer perceptron.
MLPRelu	Multilayer perceptron with Relu as activation function.

Manuscript received 20 February 2022; accepted 2 November 2022. Date of publication 17 November 2022; date of current version 29 December 2022. This work was supported in part by the Beijing Municipal Natural Science Foundation under Grant 4212012 and in part by the Fundamental Research Funds for the Central Universities under Grant YWF-19-BJ-J-307, Grant YWF-19-BJ-J-82, and Grant YWF-22-L-835. An earlier version of this article was presented at the FLEPS Conference and was published in its Proceedings [DOI: 10.1109/FLEPS51,544.2021.9,469,850]. This is an expanded paper from the IEEE SENSORS 2021 Conference. The associate editor coordinating the review of this article and approving it for publication was Dr. Hari P. Gupta. *(Corresponding author: Yang Gao.)*

Xin Ma, Xingwen Fu, and Nan Wang are with the School of Instrumentation and Optoelectronic Engineering, Beihang University (BUAA), Beijing 100191, China (e-mail: maxin@buaa.edu.cn; fu_xingwen@buaa.edu.cn; nanwang@buaa.edu.cn).

Yiqi Sun is with the Institutes of Brain Science, Fudan University, Shanghai 200032, China (e-mail: 22211520041@m.fudan.edu.cn).

Yang Gao is with the School of Physics, Beihang University (BUAA), Beijing 100089, China (e-mail: yanggao@buaa.edu.cn).

Digital Object Identifier 10.1109/JSEN.2022.3221779

MLPSig	Multilayer perceptron with Sigmoid as activation function.
MLPTSig	Multilayer perceptron with Tanh and Sigmoid as activation function.
MRI	Magnetic resonance imaging.
NIST	National Institute of Standards and Technology.
PloyECG	PolyFit-based ECG parameterization algorithm.
PTB	Physikalisch Technische Bundesanstalt.
ResNet	Residual network.
RNN	Recurrent neural network.
Sn	Sensitivity.
Sp	Specificity.
ST-Net	Spark-trace network.
SVM	Support vector machine.
TN	True negative.
TP	True positive.
TPR	Recall rate or true positive rate.
WHO	World Health Organization.

I. Introduction

ACCORDING to WHO's GHE [2], heart disease has been the leading cause of death in the world over the past 20 years. More people die of heart disease than ever before. Since 2000, the number of deaths from heart disease has increased by more than two million, to nearly nine million in 2019. Heart disease now accounts for 16% of all deaths. CHD is the most common heart disease. It refers to myocardial dysfunction and/or organic disease caused by coronary artery stenosis and insufficient blood supply, so it is also called IHD. MI is one of the most serious CHDs, which can be diagnosed by ECG, MRI, echocardiography, CK-MB, troponin, myoglobin, and magnetocardiogram (MCG) [3], [4], [5], [6], [7], [8]. In practice, it is very important to diagnose MI in time. Therefore, ECG is the first choice for patients in urgent need [9], [10], [11]. Ambulance and emergency rooms are generally equipped with ECG machines.

Cardiologists often determine the type of heart disease by observing the waveform changes of ECG signals [12], [13], [14], [15]. However, this common method also has some disadvantages. First, there is a massive imbalance between the number of cardiologists and patients. In addition, the clinical identification of MI depends on the experience of cardiologists [16]. For some atypical ECGs, less experienced physicians may not be able to make an accurate diagnosis [17]. Moreover, the speed of manual detection is slow (5–10 min/person). Therefore, automatic diagnosis of heart disease is an important branch of the medical Internet of Things [18].

There are two main machine learning methods including traditional machine learning and end-to-end deep learning to diagnose automatically [19], [20].

Traditional machine learning includes feature engineering and classifiers. Feature engineering includes discrete wavelet transform, multiscale energy and feature space, HMMs, and Fourier–Bessel series expansion. Classifiers include SVMs and KNNs [21], [22], [23], [24], [25]. If the features obtained by feature engineering have sufficient discrimination, this method can obtain high diagnostic accuracy with low computational cost. Chang et al. [26] first adopted HMMs to extract the 4-D feature vector. Then, GMMs and SVM are trained, respectively. Sharma et al. [27] obtained 96.83% diagnostic accuracy with multiscale energy and feature space and SVM. However, due to the limited level of human knowledge and experience, it is often difficult for feature engineering to obtain features with sufficient discrimination. In addition, feature engineering requires manual intervention, which makes the method cumbersome.

End-to-end deep learning integrates feature engineering into neural network, so it allows the original signal to be directly fed into the diagnostic model after simple noise reduction pretreatment [28], [29], [30], [31], [32]. It constructs high-level features through global/local modeling of information, respectively. Then, the class probability of the target is calculated according to the high-level features. The limitation of human knowledge level is avoided, so the neural network has a high upper limit of accuracy. Deep learning models such as ResNet [33] and ST-Net [34] are used to detect and localize MI. Liu et al. [32] proposed a novel MFB-CNN that can fully utilize the integrity and diversity of the ECG by using each lead of the 12-lead ECG as an independent feature branch. Then, fully connected layers are used to summarize all feature branches. However, deep features mean higher computational costs. Due to too much reliance on deep features, deep learning methods are computationally expensive in most cases.

Therefore, this article is devoted to transforming high computational cost deep features into low computational cost shallow feature logic, thereby improving speed without compromising accuracy.

To summarize, our contributions are two folds.

1) By improving DD [35], we get CDD. CDD improves the expressiveness from the potential logical relationship between features, so that smaller networks have the same accuracy as large networks.
2) As the convolution check in CDD is more sensitive to image features, we use the Hilbert curve to encode ECG signals belonging to 1-D tensor into image signals. Hilbert curve coding adopts a double recursive algorithm, which has a faster calculation speed than other mapping methods.

The rest of this article is organized as follows. Section II presents an overview of the dataset that is used in this research. Section III is dedicated to our method, providing a comprehensive explanation of the proposed framework for detecting MI. Section IV gives the results of the model and evaluates and discusses the performance of the model. Finally, Section V concludes this article with future research directions.

II. Datasets and Materials

A. Physikalisch-Technische Bundesanstalt Dataset

PTB [36] contains a total of 549 ECG data. Of the 549 records, 148 subjects are marked as MI cases, and the number of subjects marked as healthy cases is 52 (80 records). Other subjects are labeled as having heart disease unrelated to MI, such as branch block, and are therefore excluded

from this study. In this study, 20 ECG signal segments are extracted from each subject, each segment containing a heartbeat signal. Finally, a dataset containing 4000 heartbeat segments is obtained.

Due to the small number of data samples contained in this dataset, k-fold cross validation is adopted to verify the model. In order to compare with other methods under the same conditions, a fivefold cross validation method is used to validate the performance of the model [27], [33], [34], [37]. The dataset is divided as follows. First, the MI samples are taken as a positive example, and the health samples are taken as a negative example. Then, according to EasyEnsemble [38], the majority samples are under-sampled five times, and the minority samples are repeatedly sampled five times. Finally, five data subsets are obtained by combining them with each other. EasyEnsemble reduces the possibility of biased decisions. The unsampled data are used as the test set.

B. PTB-XL Datasets

The PTB-XL [39] dataset comprises 21 837 clinical 12-lead ECG records of 10-s length from 18 885 patients. From the 21 837 data, 9083 samples are marked as healthy and 2538 are marked as MI. Other cardiac diseases not related to MI are excluded from this study. Since a single recording is only 10 s, five ECG signal segments are extracted from each subject. Finally, a dataset of 11 621 heartbeat segments is obtained.

The dataset has a large number of samples, but there is also a class imbalance problem. Therefore, the minority class samples are repeatedly sampled. Unsampled data were used as a test set. The ratio of training to test is 7:1.

Note that PTB and PTB-XL are completely uncertain and public. Therefore, no ethics statement is obtained for this investigation.

C. Other Datasets

MNIST and Fashion-MNIST are used in this study to verify the performance of CDD. MNIST [40] comes from the NIST. MNIST [40] contains 70 000 images of 28 × 28 pixels. The number of classes is 10. The ratio of training and test is 6:1. Fashion-MNIST [41] shares the same data volume, data partitioning method, and data categories as MNIST. Unlike MNIST, Fashion-MNIST is no longer abstract symbols, but more concrete human necessities (clothing).

III. Methodology

An automatic detection method for MI is proposed in this article. Fig. 1 represents a simplified diagram of the method. In this method, the ECG signals are first denoised and split by preprocessing program. Then, it is encoded as image signals by the Hilbert curve. Finally, CDD Net is used to classify the image signals. The details are discussed in Sections III-A–III-C.

A. Hilbert Curve

Hilbert curve [42], a well-known space-filling curve, can traverse every pixel in the image with an uninterrupted curve while ensuring two neighbor points in the curve is also neighboring in image. A curve is a continuous mapping from [0,1] to R^2. Hilbert curve is also such a mapping. Hilbert curve is regarded as a surjection from [0,1] to region [0,1] × [0,1]. Given a point (x_0, y_0) on the unit square of the plane, we can find a parameter t_0 so that $H(t_0) = (x_0, y_0)$. The Hilbert curves of each order are shown in Fig. 2. The double recursive implementation of the Hilbert curve is shown in Table I.

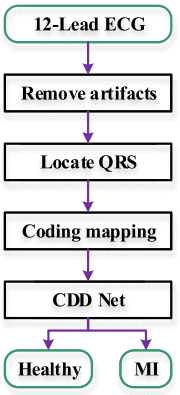

Fig. 1. Flowchart of MI automatic detection method.

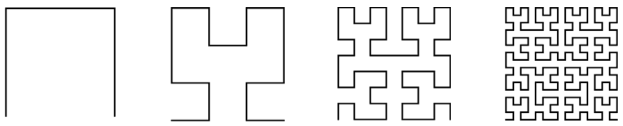

Fig. 2. Hilbert curves of various orders. From left to right are first-, second-, third-, and fourth-order Hilbert curves.

TABLE I
Double Recursive Implementation of Hilbert Curve Coding (Python)

```
# N is the order
# L is the step size
# right (90) is rotate 90 degrees to the right
# left (90) is rotate 90 degrees to the left
```

Clockwise rotation	Counterclockwise rotation
`def hilL(n):`	`def hilR(n):`
`  if n==0:`	`  if n==0:`
`  pass`	`  pass`
`  if n>0:`	`  if n>0:`
`  right(90)`	`  left(90)`
`  hilR(n-1)`	`  hilL(n-1)`
`  forward(L)`	`  forward(L)`
`  left(90)`	`  right(90)`
`  hilL(n-1)`	`  hilR(n-1)`
`  forward(L)`	`  forward(L)`
`  hilL(n-1)`	`  hilR(n-1)`
`  left(90)`	`  right(90)`
`  forward(L)`	`  forward(L)`
`  hilR(n-1)`	`  hilL(n-1)`
`  right(90)`	`  left(90)`

```
def main():
  hilL(n=4)
```

B. Data Processing

1) Original ECG Signal: The original ECG signal is shown in Fig. 3(a).

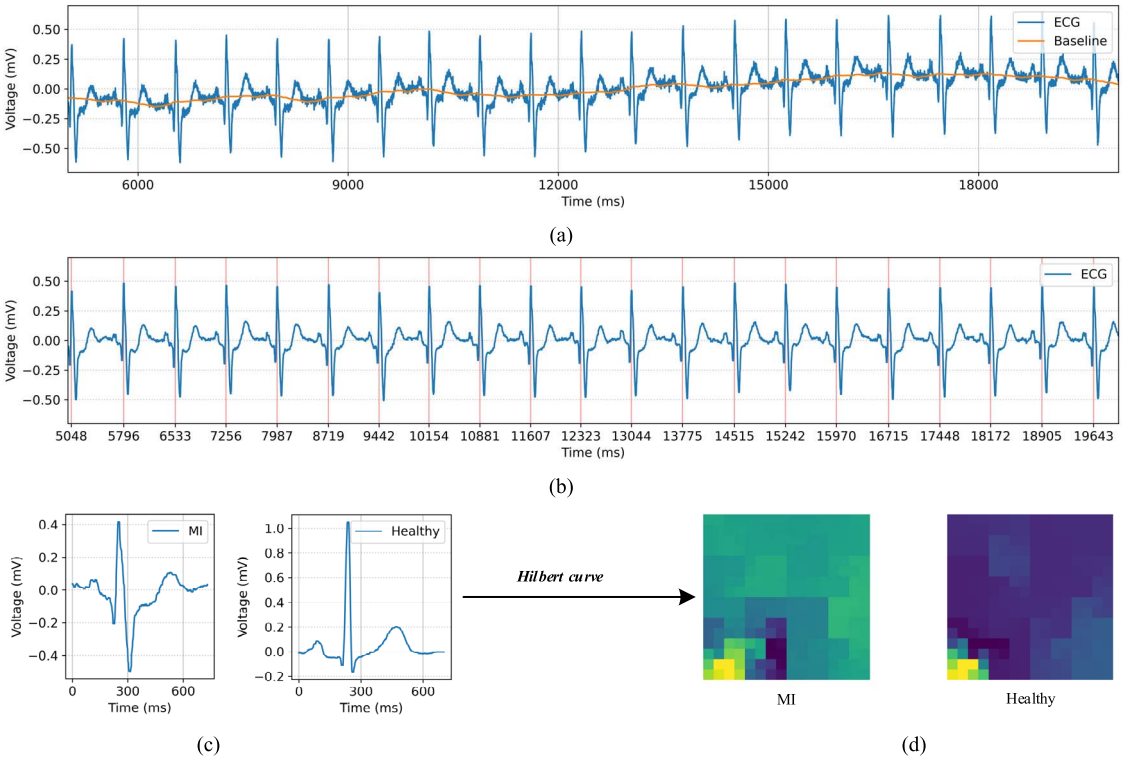

Fig. 3. Data processing. (a) Original ECG signal. (b) ECG signal after artifact removal. (c) ECG signal of heartbeat. (d) Image signal encoded by Hilbert curve.

a) Remove artifacts: The ECG signal might be destroyed by two main artifacts. First, BW may be caused by the movement and breathing of patients or instruments' instability recording the ECG signal. The frequency of the BW is between 0.05 and 5 Hz, with the main component around 0.1 Hz. However, ECG has information from 0.5 to 5 Hz (low-frequency components of T-wave and P-wave). The T-wave component is extremely important for MI detection. Therefore, a median filter is used to obtain the baseline of the original signal, as shown in Fig. 3(a). The baseline includes the drift of the original signal. Baseline is subtracted from the original signal to eliminate BW. Second, high-frequency noise, such as the noise caused by EMG, the mechanical force on the electrode, and power line interference [36]. Low-pass filters with 60 Hz [33] are used to suppress high-frequency noise. The ECG signal after noise reduction is shown in Fig. 3(b).

b) Locate QRS complex: QRS complex localization algorithm is follows [37]. From the ECG, QRS complex has the characteristics of steep slope and sharp change. First, the position of the R peak is located by the differential threshold method, as shown by the red grid line in Fig. 3(b), and then the position is used as the reference point to intercept a complete heartbeat signal. A complete heartbeat signal is illustrated in Fig. 3(c).

c) Code by Hilbert curve: After artifact removal and location splitting of the data, the ECG signal, which belongs to the time series, is transformed into image signal. The Hilbert curve is used to complete the transformation process. On the premise that the time-domain characteristics of ECG signal are not destroyed, the calculation cost is considered in this study. Hence, each sample under each channel of the original data is sampled with a fixed length of 256 data points. Then, the ECG signal is encoded into image signal by a fourth-order Hilbert curve, as shown in Fig. 2(d).

C. Classifier

Traditional ANNs complete feature extraction and classification surface construction by embedding nonlinear activation functions in linear networks. They construct high-level features through global/local modeling of information, respectively. Then, the class probability of the target is calculated according to the high-level features. However, due to too much reliance on deep features, the computational cost is high. It can be simply described as follows:

$$\boldsymbol{X}^{k+1} = F^k\left(\boldsymbol{X}^k \otimes \boldsymbol{W}^k + \boldsymbol{B}^k\right) \tag{1}$$

where k is the layer mark, $\boldsymbol{X}$ is the feature map, $F(\cdot)$ is the nonlinear activation function, $\boldsymbol{W}$ is the weight matrix of convolution layer, and $\boldsymbol{B}$ is the bias matrix.

Simulating the functions of biological dendrites [43], Liu Gang et al. [35] designed DD and further developed it into Gang neuron [44]. For DD, some advantages of ANN are that: 1) consider the logical relationship of input data and 2) use dendrite as a replacement for the nonlinear activation function of ANN, which obtains a white-box model. The number of dendrite layers can be altered with a purpose based on the results of its classification or fitting. Therefore, DD could effectively reduce overfitting or underfitting from the networks which are too deep or shallow. DD achieves good results on classification datasets, such as MNIST and Fashion-MNIST.

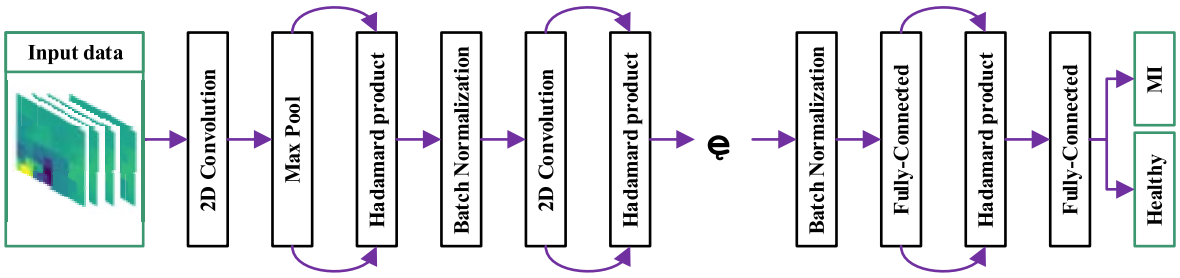

Fig. 4. CDD Net structure. There are 12 channels of input data. The number of CDDs is 5. CDD Net only contains a nonlinear activation function softmax in the output layer.

The mathematical model of DD networks is shown as follows:

$$\boldsymbol{X}^{k+1} = \left(\boldsymbol{X}^k \boldsymbol{W}^k\right) \circ \boldsymbol{X} \tag{2}$$

where k is the layer mark, $\boldsymbol{X}$ is the logic map, $\boldsymbol{W}$ is the weight matrix, and $\circ$ is the *Hadamard product*.

However, the following two problems are still challenging.

1) DD lacks the weight sharing, inductive bias, and translation invariance inherent in CNNs.
2) There is a dimension mismatch in the process of data propagation.

Hence, in response to the above two problems, CDD is proposed. The mathematical model of CDD is shown in (3). The addition of convolution brings important weight sharing, inductive bias, and translation invariance to the model. The calculation of autocorrelation logic avoids the dimension mismatch in the process of data propagation. In addition, the mathematical model of CDD is simple and beautiful, and programming is also simple. Only one line of code X = (W⊗X)*(W⊗X) (python) is given

$$\boldsymbol{X}^{k+1} = \left(\boldsymbol{X}^k \otimes \boldsymbol{W}^k + \boldsymbol{B}^k\right) \circ \left(\boldsymbol{X}^k \otimes \boldsymbol{W}^k + \boldsymbol{B}^k\right) \tag{3}$$

where k is the layer mark, $\boldsymbol{X}$ is the logic map, $\boldsymbol{W}$ is the weight matrix, $\boldsymbol{B}$ is the bias matrix, and $\circ$ is the *Hadamard product*.

CDD is transplanted to MI automatic detection method and constructed a relatively simple classification model called CDD Net, as shown in Fig. 4. CDD Net includes five CDDs, and the batch normalization layer is used between every two CDDs. The role of normalization is to avoid data overflow caused by accumulation. The max pooling layer in the first CDD is used to eliminate data that does not contribute to classification. In the last CDD, the convolution layer is modified to a fully connected layer, and then the Hadamard product is used to comprehensively consider the whole extracted features. The full connection layer can be regarded as convolution operation handling convolution kernel with the same size as the input data. Thus, it is still identified as CDD in this article. Except for the softmax in the output layer, the other layers do not contain nonlinear activation functions. In this article, CDD Net is used to classify the image data encoded by the Hilbert curve. The results are detailed in Section IV.

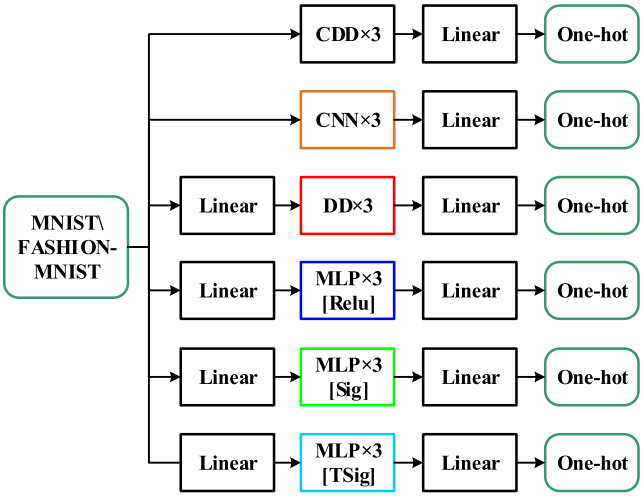

Fig. 5. Model framework; CNN and MLP with different activation functions are ANN, DD is traditional Dendrite Net, and CDD is the model proposed in this article.

IV. Results and Discussion

In order to make a comprehensive and accurate evaluation of the whole method, this section is divided into the following two parts. The first part shows the comparison results of CDD with the current classification models on MNIST and Fashion-MNIST datasets. In the second part, the performance of the MI automatic detection method on the PTB dataset is compared with some existing models in this field. Meanwhile, ablation experiments are performed on PTB-XL.

A. MNIST and Fashion-MNIST Dataset

As mentioned earlier, MNIST contains 70 000 handwritten numeral images, and Fashion-MNIST dataset contains 70 000 images of various clothing types, of which 60 000 are used for training and 10 000 for prediction. Fig. 6 shows the detailed framework of the experimental group and the control group. CDD is the experimental group, and the rest make up the control group, including CNN, DD, and MLP with different activation functions [such as Relu, sigmoid (Sig), tanh, and sigmoid (Tsig)]. For comparison, all models have similar structures, as shown in Fig. 5.

The experimental results are reported in Fig. 6. CDD has higher test accuracy and lower training error. Compared with traditional classification models, CDD enhances the expressiveness of neural networks. In addition, CDD has a

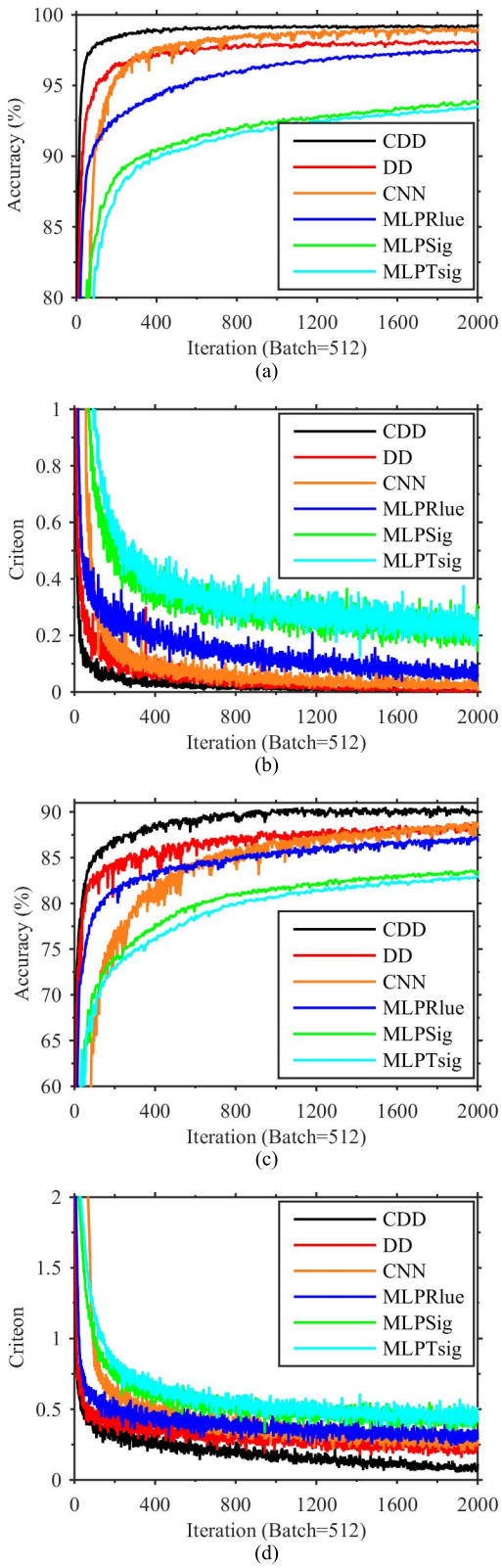

Fig. 6. Validation results. (a) and (b) Rising curve of accuracy and the falling curve of error using MNIST dataset. (c) and (d) Rising curve of accuracy and the falling curve of error using Fashion-MNIST dataset.

faster convergence rate, which means that the training process of the model is more efficient. The convergence rate can be obtained from the slope of the accuracy curve and the error curve during the convergence process. The analysis of the above two phenomena is as follows.

CDD absorbs the advantages of local perception and weight sharing of CNN. Local perception is that each neuron does not need to perceive all the pixels in the image, only perceives the local pixels of the image, and then combines this local information at a higher level to obtain all the representation information of the image. Weight sharing is similar to biological neural network, which reduces the complexity of the network model and the number of weights [45], [46]. This network structure is highly invariant to translation, scaling, tilting, or other forms of deformation. Local sensing ensures that the learned convolution check has the strongest response to the input spatial local pattern. Weight sharing ensures that the model achieves higher performance with smaller parameters.

CDD inherits the characteristics of DD's construction of logical relationships. In addition, because of the existence of bias matrix, CDD retains the shallow logic relationship. CDD not only extracts the features of input data but also their logical relationship at the same time. In the classification, CDD pays more attention to the combination of features.

B. PTB and PTB-XL Dataset

In this section, PTB and PTB-XL are used to test the performance of CDD Net. As mentioned earlier, 4000 ECG segments are obtained from PTB and 11 621 ECG segments are obtained from PTB-XL. Compared with PTB, the data situation of PTB-XL is more complicated. The classification model includes the following performance indicators, as shown in the following equation:

$$\text{Acc} = \frac{\text{TP} + \text{TN}}{\text{TP} + \text{FN} + \text{TN} + \text{FP}} \tag{4}$$

$$\text{Sn} = \frac{\text{TP}}{\text{TP} + \text{FN}} \tag{5}$$

$$\text{Sp} = \frac{\text{TN}}{\text{TN} + \text{FP}} \tag{6}$$

where Acc (accuracy) is the ratio of the correct forecast to the total forecast. Sn (sensitivity), also known as recall rate or TPR, measures the proportion of positive predictions correctly identified in all positive cases. Sp (specificity), also known as TNR, is an indicator to correctly identify the proportion of negative predictions. TP, FP, TN, and FN represent true positive, false negative, true negative, and false positive, respectively. The confusion matrix of these four cases is shown in Table II.

1) Implementation: Pytorch is used to implement the CDD Net described in Fig. 4. All adjustable parameters are initialized randomly. The multiclass cross entropy loss function is taken as the optimization objective, and the model is iterated 500 times. The optimizer is Adam's learning rate is 5e−4, weight decay is 1e−5, and other parameters are the default values. The branch training method is used to train the model. Each branch has 900 samples.

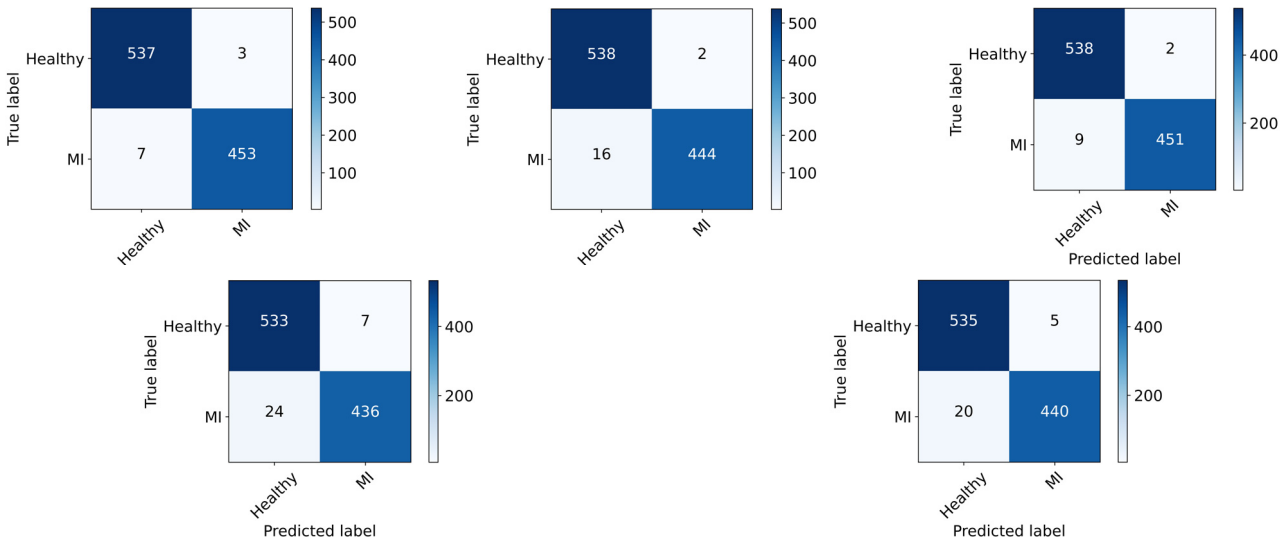

Fig. 7. Confusion matrices; From left to right and top to bottom: confusion matrices from the first, second, third, fourth, and fifth cross-validation folds.

TABLE II
MODEL EVALUATION INDEX BY CONFUSION MATRIX

True Label	Predicted Label	
	Positive (MI Label=1)	Negative (Normal Label=0)
Positive (MI Label=1)	TP	FN
Negative (Healthy Label=0)	FP	TN

TABLE III
EVALUATION RESULTS OF MI AUTOMATIC DETECTION METHODS

Performance metric	Fold 1	Fold 2	Fold 3	Fold 4	Fold 5	Average
Accuracy (%)	99.00	99.52	98.93	97.63	97.52	98.52
Sensitivity (%)	98.47	99.78	98.04	96.15	95.65	97.62
Specificity (%)	99.44	99.26	99.62	98.14	99.07	99.11

2) Performance: The performance of the model is shown in Table III and Fig. 7. The average MI detection accuracy, sensitivity, and specificity were 98.52%, 97.62%, and 99.11%, respectively. Fig. 7 more intuitively shows that the model has a lower probability of biased decision-making. To intuitively reflect the performance of the MI automatic detection method, Table IV provides a summary of the literature on MI detection. To avoid differences in precision from chance factors, the precision of **P.M.** in Table IV is the mean of five replicate experiments. PTB dataset is used as data sources in this literature. Table IV compares the diagnosis time, specificity, sensitivity, and accuracy between the proposed algorithm and the existing algorithms, and lists the corresponding hardware resources. Under common hardware conditions, CDD Net reduces computation time without compromising detection accuracy. As it can improve the performance from the potential logical relationship between features, CDD Net is smaller than the traditional deep learning model with large parameters. It achieves or even exceeds the diagnostic accuracy of the traditional model with relatively low hardware cost, which is of great significance in practical application.

TABLE IV
LITERATURE INDEX OF AUTOMATIC DETECTION OF MI

Ref.	Model	Hardware	Time (ms)	MI (%)		
				Sp	Sn	Acc
[27]	MEMS	Intel i5 processor @3.20 GHz CPU, 4-GB RAM	440.00	99.00	93.00	96.00
[34]	ST-Net	RTX 2080TI GPU	300.00	98.09	98.19	98.13
[28]	DCNN	-	-	94.19	95.49	95.22
[46]	CNN & RNN	Intel Core i5-4590 @3.3GHz CPU, 8G RAM, GTX 750 GPU	60.00	86.50	98.20	95.40
[47]	PolyECG	-	-	-	-	94.40
[37]	CNN	Intel Core i7-3770 @ 3.4 GHz CPU, 12 GB RAM, No GPU	17.10	97.37	95.40	96.00
[48]	EDN	-	-	98.95	-	98.88
[49]	ARB-Net	Intel Core i5-4590 @3.3GHz CPU, 16GB RAM, Quadro K600 GPU	8.42	99.20	97.60	98.30
P.M.	**CDD Net**	Intel (R) Xeon (R) platinum 8163 @ 2.50GHz CPU 8GB RAM, NVIDIA Tesla T4 GPU	**2.09**	**99.11**	**97.62**	**98.52**
		No GPU	**5.88**			

Sn: Sensitivity, Sp: Specificity, Acc: Accuracy, **P.M.: Proposed Method.**

The precision of **P.M.** is the mean of 5 replicate experiments.

(-) indicates the information that is not reported in the original study or could not be computed from the study.

TABLE V
ABLATION EXPERIMENTS PERFORMED ON PTB-XL

Name	# Params	Sp(%)	Sn(%)	Acc(%)
DD	4.28M	95.01	92.36	94.21
CNN+Resize	0.91M	93.05	86.95	91.57
CDD Net+Resize	0.91M	93.65	87.01	92.21
CNN+Hilbert curves	0.91M	93.70	93.33	93.64
CDD Net+Hilbert curves	**0.91M**	**97.23**	**95.23**	**96.80**

Params is the amount of model parameters;
CNN, DD and CDD have the same architecture and optimization scheme.

3) Computational Complexity: The trained model is embedded into the automatic diagnosis method. In order to comprehensively evaluate the hardware resource occupation and running speed of this method, we calculate the parameters, computational complexity, and computational time of the whole method. The GPU model is NVIDIA Tesla T4, and the CPU model is Intel (R) Xeon (R) platinum 8163 CPU at 2.50 GHz. The parameters of the whole model are 0.91 MB and the computational complexity is 1.68 Mflops. The calculation time of a single patient is 2.09 ms. Diagnosis process of a single patient includes artifact removal, QRS complex positioning, coding mapping, and 20 beat signal recognition. If only CPU is used, the calculation time is 5.88 ms. It should be noted that the automatic diagnosis method proposed in this article can achieve high speed and high precision prediction under the condition of low hardware configuration.

4) Ablation Experiment: To find the source of the performance improvement, PTB-XL is used to perform ablation experiments. CDD, CNN, and DD are used for testing. In order to conduct experiments objectively, all networks have similar structures, the same artifact removal methods, and optimization schemes. The experimental results are reported in Table V. To avoid differences in precision caused by chance factors, all results in Table V are the average of five experiments. From Table V, the following holds.

1) *Comparing CDD and CNN:* Under the same architecture, optimization, and parameters, just replacing the CNN with CDD Net can get the accuracy improvement.
2) *Compare Resize and Hilbert curves*: If the time-series signal is simply resized into an image signal, the performance is degraded due to the destruction of the time-domain features. Therefore, guaranteeing a complete mapping of temporal features to image features during data processing is crucial for subsequent classification.
3) *Processing the Timing Signals Directly by Using DD Seems to Have Good Results:* However, the fully connected structure leads to a relatively large amount of parameters in DD.

V. CONCLUSION

Timely diagnosis of MI is essential to save lives. In order to detect MI accurately and quickly, an automatic detection method based on ECG signal is proposed. In this method, after preprocessing, the ECG signal is encoded to the image by Hilbert curve, and then the image is sent to the CDD Net proposed in this article for diagnosis. The average accuracy of the model is 98.52% (fivefold cross validation). And the detection time of a single patient only needs 2.09 ms, which is of great significance for MI diagnosis. Similarly, the whole algorithm has ultralow computational complexity (1.68 Mflops) and parameters (0.91 MB), which makes it possible to embed small wearable devices. Our MI automatic detector is superior to other report classifiers using the same dataset.

Two advantages of the model are summarized as follows. First, the Hilbert curve makes it possible to apply a computer vision model to time-series signal. The coding process inherits the advantages of the Hilbert curve. The time-domain feature of ECG signal is almost completely transformed into the shape feature of the image signal. Second, CDD is more expressive, portable, and efficient. CDD absorbs the advantages of DD and CNN. It extracts features and the logical relationship between features at the same time and pays more attention to the combination of features in classification.

There is a shortcoming in that the Hilbert curve encoding is discontinuous, and the high-frequency signal is slightly lost during fixed-length sampling. But since the high-frequency part is mostly noise, this does not affect the accuracy of the method.

The method proposed in this article may have other applications. In the field of automatic diagnosis of heart disease, it is expected to obtain cardiac magnetic signal with the help of high-precision cardiac magnetic sensing equipment in the future, so as to realize the rapid diagnosis and positioning of heart disease. In the field of artificial intelligence, the Hilbert curve is classic and practical. It can not only map ECG signals to image signals, but also build an efficient bridge between computer vision and other time series signals in the future. CDD is simple, efficient, and transplantable. As a general classification module, CDD not only achieves remarkable results in the automatic detection of MI but also has broad development potential in other kinds of image recognition projects in the future.

ACKNOWLEDGMENT

The authors would like to thank Prof. Xiaolin Ning, Assoc. Prof. Min Xiang, and all other members of the Key Laboratory of Ultra-Weak Magnetic Field Measurement Technology, Ministry of Education, for their useful comments on this work.

REFERENCES

[1] X. Ma, X. Fu, Y. Sun, N. Wang, X. Ning, and Y. Gao, "Convolutional dendrite net detects myocardial infarction based on ECG signal measured by flexible sensor," in *Proc. IEEE Int. Conf. Flexible Printable Sensors Syst. (FLEPS)*, Jun. 2021, pp. 1–4.
[2] *Global Health Estimates*. Accessed: Apr. 26, 2021. [Online]. Available: https://www.who.int/data/global-health-estimates
[3] B. Lavin et al., "MRI with gadofosveset: A potential marker for permeability in myocardial infarction," *Atherosclerosis*, vol. 275, pp. 400–408, Aug. 2018.
[4] Z. M. Hijazi and H. Suradi, "Intracardiac echocardiography-guided interventions: Do we need trials to prove equivalency/superiority to transesophageal echocardiography?" *JACC, Cardiovascular Intervent.*, vol. 7, no. 9, pp. 1045–1047, Sep. 2014.

[5] C. Eek et al., "Strain echocardiography and wall motion score index predicts final infarct size in patients with non–ST-segment–elevation myocardial infarction," *Circulat., Cardiovascular Imag.*, vol. 3, no. 2, pp. 187–194, Mar. 2010.

[6] A. Bagai et al., "Prognostic implications of creatine kinase–MB measurements in ST-segment elevation myocardial infarction patients treated with primary percutaneous coronary intervention," *Amer. Heart J.*, vol. 168, no. 4, pp. 503–511, Oct. 2014.

[7] J. A. Wang, Y. Qin, J. Lv, Y. F. Tian, and Y. J. Dong, "Clinical application of high-sensitivity cardiac troponin T test in acute myocardial infarction diagnosis," *Genet. Mol. Res.*, vol. 14, no. 4, pp. 17959–17965, 2015.

[8] Y. Yang et al., "A new wearable multichannel magnetocardiogram system with a SERF atomic magnetometer array," *Sci. Rep.*, vol. 11, Mar. 2021, Art. no. 5564.

[9] L. Lambert, K. Brown, E. Segal, J. Brophy, J. Rodes-Cabau, and P. Bogaty, "Association between timeliness of reperfusion therapy and clinical outcomes in ST-elevation myocardial infarction," *J. Amer. Med. Assoc.*, vol. 303, pp. 55–2148, Jun. 2010.

[10] T. Verulava, T. Maglakelidze, and R. Jorbenadze, "Hospitalization timeliness of patients with myocardial infarction," *Eastern J. Med.*, vol. 22, no. 3, pp. 103–109, 2017.

[11] C. D. Cantwell et al., "Rethinking multiscale cardiac electrophysiology with machine learning and predictive modelling," *Comput. Biol. Med.*, vol. 104, pp. 339–351, Jan. 2019.

[12] Y. Cao et al., "ML-Net: Multi-channel lightweight network for detecting myocardial infarction," *IEEE J. Biomed. Health Informat.*, vol. 25, no. 10, pp. 3721–3731, Oct. 2021.

[13] S. Saadatnejad, M. Oveisi, and M. Hashemi, "LSTM-based ECG classification for continuous monitoring on personal wearable devices," *IEEE J. Biomed. Health Informat.*, vol. 24, no. 2, pp. 515–523, Feb. 2020.

[14] N. Strodthoff, P. Wagner, T. Schaeffter, and W. Samek, "Deep learning for ECG analysis: Benchmarks and insights from PTB-XL," Apr. 2020, *arXiv:2004.13701*. Accessed: Apr. 25, 2021.

[15] X. Fan, Q. Yao, Y. Cai, F. Miao, F. Sun, and Y. Li, "Multiscaled fusion of deep convolutional neural networks for screening atrial fibrillation from single lead short ECG recordings," *IEEE J. Biomed. Health Informat.*, vol. 22, no. 6, pp. 1744–1753, Nov. 2018.

[16] Y. H. Awni et al., "Cardiologist-level arrhythmia detection and classification in ambulatory electrocardiograms using a deep neural network," *Nature Med.*, vol. 25, pp. 65–69, Jan. 2019.

[17] A. D. Arnold et al., "Discriminating electrocardiographic responses to his-bundle pacing using machine learning," *Cardiovascular Digit. Health J.*, vol. 1, no. 1, pp. 11–20, Jul. 2020.

[18] K. G. Pollock et al., "Application of a machine learning algorithm for detection of atrial fibrillation in secondary care," *IJC Heart Vasculature*, vol. 31, Dec. 2020, Art. no. 100674.

[19] A. S. Panayides et al., "AI in medical imaging informatics: Current challenges and future directions," *IEEE J. Biomed. Health Informat.*, vol. 24, no. 7, pp. 1837–1857, Jul. 2020.

[20] X. Li, B. S. Handa, N. S. Peters, and F. S. Ng, "Classification of fibrillation subtypes with single-channel surface electrocardiogram," in *Advances in Computational Intelligence Systems*. Cham, Switzerland, 2020, pp. 472–479.

[21] H. Moosaei, S. Ketabchi, M. Razzaghi, and M. Tanveer, "Generalized twin support vector machines," *Neural Process. Lett.*, vol. 53, no. 2, pp. 1545–1564, Apr. 2021.

[22] H. Fang, D. Hu, Q. Li, and S. Tu, "Risk gene identification and support vector machine learning to construct an early diagnosis model of myocardial infarction," *Mol. Med. Rep.*, vol. 22, no. 3, pp. 1775–1782, Jun. 2020.

[23] S. S. Kasim, S. Malek, K. K. S. Ibrahim, and M. F. Aziz, "Risk stratification of Asian patients after ST-elevation myocardial infarction using machine learning methods," *Eur. Heart J.*, vol. 41, Nov. 2020, Art. no. ehaa946.

[24] C. Xu, L. Xu, H. Zhang, Y. Zhang, X. Du, and S. Li, "A novel machine-learning algorithm to estimate the position and size of myocardial infarction for MRI sequence," *Computing*, vol. 101, no. 6, pp. 653–665, Jun. 2019.

[25] M. Kumar, R. Pachori, and U. Acharya, "Automated diagnosis of myocardial infarction ECG signals using sample entropy in flexible analytic wavelet transform framework," *Entropy*, vol. 19, no. 9, p. 488, Sep. 2017.

[26] P.-C. Chang, J.-J. Lin, J.-C. Hsieh, and J. Weng, "Myocardial infarction classification with multi-lead ECG using hidden Markov models and Gaussian mixture models," *Appl. Soft Comput.*, vol. 12, no. 10, pp. 3165–3175, Oct. 2012.

[27] L. N. Sharma, R. K. Tripathy, and S. Dandapat, "Multiscale energy and eigenspace approach to detection and localization of myocardial infarction," *IEEE Trans. Biomed. Eng.*, vol. 62, no. 7, pp. 1827–1837, Jul. 2015.

[28] U. R. Acharya, H. Fujita, S. L. Oh, Y. Hagiwara, J. H. Tan, and M. Adam, "Application of deep convolutional neural network for automated detection of myocardial infarction using ECG signals," *Inf. Sci.*, vols. 415–416, pp. 190–198, Nov. 2017.

[29] A. Rogers et al., "Deep neural network trained on surface ECG improves diagnostic accuracy of prior myocardial infarction over *Q* wave analysis," *Eur. Heart J.*, vol. 41, Nov. 2020, Art. no. ehaa946.

[30] A. Shaker, M. Tantawi, H. Shedeed, and M. Tolba, "Combination of convolutional and recurrent neural networks for heartbeat classification," in *Proc. Int. Conf. Artif. Intell. Comput. Vis.*, 2020, pp. 362–371.

[31] D. Rajan, D. Beymer, and G. Narayan, "Generalization studies of neural network models for cardiac disease detection using limited channel ECG," Jan. 2019, *arXiv:1901.03295*. Accessed: Apr. 25, 2021.

[32] W. Liu, Q. Huang, S. Chang, H. Wang, and J. He, "Multiple-feature-branch convolutional neural network for myocardial infarction diagnosis using electrocardiogram," *Biomed. Signal Process. Control*, vol. 45, pp. 22–32, Aug. 2018.

[33] K. Jafarian, V. Vahdat, S. Salehi, and M. Mobin, "Automating detection and localization of myocardial infarction using shallow and end-to-end deep neural networks," *Appl. Soft Comput.*, vol. 93, Aug. 2020, Art. no. 106383.

[34] Y. Deng et al., "ST-Net: Synthetic ECG tracings for diagnosing various cardiovascular diseases," *Biomed. Signal Process. Control*, vol. 61, Aug. 2020, Art. no. 101997.

[35] G. Liu and J. Wang, "Dendrite Net: A white-box module for classification, regression, and system identification," Oct. 2020, *arXiv:2004.03955*. Accessed: Apr. 26, 2021.

[36] A. L. Goldberger et al., "PhysioBank, PhysioToolkit, and PhysioNet," *Circulation*, vol. 101, no. 23, pp. e215–e220, Jun. 2000.

[37] W. Liu et al., "Real-time multilead convolutional neural network for myocardial infarction detection," *IEEE J. Biomed. Health Informat.*, vol. 22, no. 5, pp. 1434–1444, Sep. 2018.

[38] X.-Y. Liu, J. Wu, and Z.-H. Zhou, "Exploratory undersampling for class-imbalance learning," *IEEE Trans. Syst., Man, Cybern. B, Cybern.*, vol. 39, no. 2, pp. 539–, Apr. 2009.

[39] P. Wagner et al., "PTB-XL, a large publicly available electrocardiography dataset," *Sci. Data*, vol. 7, p. 154, May 2020.

[40] Y. LeCun, L. Bottou, Y. Bengio, and P. Haffner, "Gradient-based learning applied to document recognition," *Proc. IEEE*, vol. 86, no. 11, pp. 2278–2324, Nov. 1998.

[41] H. Xiao, K. Rasul, and R. Vollgraf, "Fashion-MNIST: A novel image dataset for benchmarking machine learning algorithms," Aug. 2017, *arXiv:1708.07747*.

[42] G. Nguyen, P. Franco, R. Mullot, and J. Ogier, "Mapping high dimensional features onto Hilbert curve: Applying to fast image retrieval," in *Proc. 21st Int. Conf. Pattern Recognit. (ICPR)*, 2012, pp. 425–428.

[43] A. Gidon et al., "Dendritic action potentials and computation in human layer 2/3 cortical neurons," *Science*, vol. 367, no. 6473, pp. 83–87, Jan. 2020.

[44] G. Liu, "It may be time to improve the neuron of artificial neural network," *TechRxiv*, Jul. 2021, doi: 10.36227/techrxiv.12477266.v10.

[45] X. Lu, Q. Xie, Y. Zha, and D. Wang, "Fully automatic liver segmentation combining multi-dimensional graph cut with shape information in 3D CT images," *Sci. Rep.*, vol. 8, no. 1, pp. 1–9, Dec. 2018. Accessed: May 12, 2021. [Online]. Available: https://www.ncbi.nlm.nih.gov/pmc/articles/PMC6048104/

[46] Q. Dou et al., "Automatic detection of cerebral microbleeds from MR images via 3D convolutional neural networks," *IEEE Trans. Med. Imag.*, vol. 35, no. 5, pp. 1182–1195, May 2016.

[47] K. Feng, X. Pi, H. Liu, and K. Sun, "Myocardial infarction classification based on convolutional neural network and recurrent neural network," *Appl. Sci.*, vol. 9, no. 9, p. 1879, May 2019.

[48] B. Liu et al., "A novel electrocardiogram parameterization algorithm and its application in myocardial infarction detection," *Comput. Biol. Med.*, vol. 61, pp. 178–184, Jun. 2015.

[49] T. Mahmud, A. R. Hossain, and S. A. Fattah, "ECGDeepNET: A deep learning approach for classifying ECG beats," in *Proc. 7th Int. Conf. Robot Intell. Technol. Appl. (RiTA)*, Nov. 2019, pp. 32–37.

[50] E. Prabhakararao and S. Dandapat, "Attentive RNN-based network to fuse 12-lead ECG and clinical features for improved myocardial infarction diagnosis," *IEEE Signal Process. Lett.*, vol. 27, pp. 2029–2033, 2020.

Xin Ma (Member, IEEE) was born in Baotou, China, in 1985. She received the B.E. degree in electronic and communication engineering from Inner Mongolia University, Hohhot, China, in 2008, and the Ph.D. degree in precision instruments and machinery from Beijing University of Aeronautics and Astronautics (now Beihang University), Beijing, China, in 2016.

She was a Visiting Scholar with the National University of Singapore, Singapore. She is currently an Assistant Professor with the School of Instrumentation and Optoelectronic Engineering, Beihang University (BUAA). Her research interests include biomedical image processing and machine learning and classification.

Xingwen Fu was born in Nanchang, Jiangxi, China, in 1997. He received the B.S. degree in measurement and control technology and instruments from Shandong University of Technology, Shandong, China, in 2020. He is currently pursuing the M.S. degree with the School of Instrumentation and Optoelectronic Engineering, Beihang University (BUAA), Beijing, China.

His research interests include biological signal processing and computer vision.

Yiqi Sun was born in Fuyang, Anhui, China, in 2000. She received the B.S. degree in computer science and technology from Beihang University (BUAA), Beijing, China, in 2022. She is currently pursuing the M.S. degree with the Institutes of Brain Science, Fudan University, Shanghai, China.

Her research interests include neural communication and computing.

Nan Wang was born in Dezhou, Shandong, China, in 1996. He received the B.S. degree in measurement and control technology and instruments from Shandong University of Technology, Shandong, China, in 2019. He is currently pursuing the M.S. degree with the School of Instrumentation and Optoelectronic Engineering, Beihang University (BUAA), Beijing, China.

His research interests include pattern recognition and deep learning.

Yang Gao received the Ph.D. degree in instrument science and technology from Beihang University, Beijing, China, in 2018.

He is now a Postdoctoral Researcher with the School of Physics, BUAA. Before joining BUAA, he worked as an Associate Professor at the Beijing Academy of Quantum Information Sciences (BAQIS). His research interests include signal processing, multimodality biomedical imaging techniques, and machine learning.